Proceedings of the
Annual Stability Conference
Structural Stability Research Council
Toronto, Canada, March 25-28, 2014

An Alternative Approach for the Prediction of Hollow Structural Shapes Cross-sectional Resistance: the Overall Interaction Concept

J. Nseir[1], E. Saloumi[2], M. Hayeck[3], A. Taras[4], N. Boissonnade[5]

Abstract

This paper deals with the application of the Overall Interaction Concept (O.I.C.) to the practical design of hollow structural shapes. More precisely, the concern here is to demonstrate the ability of the O.I.C. to accurately account for the influence of local buckling on the cross-sectional carrying capacity. In this respect, detailed investigations have been performed, covering the various influences of i) plastic to slender cross-sectional behavior, ii) rectangular, square or circular hollow section shapes, iii) cold-formed or hot-finished elements, and iv) simple to complex loading situations.

First, the paper describes an extensive experimental program that comprised 57 main tests and reports the results on initial geometric imperfections and residual stresses measurements. This information is further used within the validation of FE shell models versus test results.

The numerical models were shown to correlate quite well with experimental results and were then employed in parametric studies aiming at characterizing the onset of local buckling with respect to the parameters listed above. Further developments are actually under way to finalize a comprehensive and consistent design procedure by using the numerical results.

1. Introduction

The present paper is related to the stability, resistance and design of steel hollow section members. More precisely, the behavior of hollow sections is investigated through a large experimental campaign of 57 tests with the intention of improving the way the performance and the carrying capacity of tubular members are actually characterized, through the development of an original "Overall Interaction Concept" (O.I.C.). Taking into account the resistance and stability interaction, the OIC further incorporates the effects of imperfections (non-homogenous material, residual stresses, out-of-straightness…) through the derivation of adequate "interaction curves" used to accurately predict the real behavior of structural elements. The proposed concept is powerful enough to i) increase accuracy and bridge the specificities of the different materials

[1] Graduate Student, University of Applied Sciences of Western Switzerland, <joanna.nseir@gmail.com>
[2] Graduate Student, University of Applied Sciences of Western Switzerland, <elsysaloumi@gmail.com>
[3] Graduate Student, University of Applied Sciences of Western Switzerland, <marielle_hayeck@hotmail.com>
[4] Assistant Professor, Graz University of Technology, <taras@tugraz.at>
[5] Professor, University of Applied Sciences of Western Switzerland, <nicolas.boissonnade@hefr.ch>

under a unified, simple and effective basis, ii) deal with the effects of non-linear material behavior and local/global instabilities, and iii) advance consistency with the possibility of straightforwardly deal with all load cases, including combined ones (Figure 1).

At present, for what regards cross-sectional instability, design codes (e.g. Eurocode 3, CEN 2005, AISC) usually characterize the sensitivity to early or late occurrence of local buckling by means of a classification of the cross-section, with respect to the b/t ratios of each wall comprised within the cross-section. Different sets of design formulae are provided, either plastic or elastic, depending on the (weakest) element, which defines the cross-section class.

This concept of classes causes many practical application difficulties, such as a gap of resistance, complicated calculations for slender sections, etc… and almost no attempts have been made to overcome this unsatisfactory situation in a global way. In particular, the classification concept was shown to be inappropriate for hollow sections (Boissonnade 2011, Gardner 2008, Semi-Comp 2007).

The aim of the present research investigations is to show how the O.I.C. can improve this situation, and to demonstrate that the O.I.C. is perfectly suited to the determination of the design resistance of hollow sections for simple load cases as well as combined cases. The following Section 2 presents the detailed experimental campaign with the corresponding preliminary measurements (tensile tests, imperfection measurements, residual stress measurements). Passing on to section 3 which presents the numerical results FEM vs. Experimental results in which the numerical model is proved to be validated and used for further parametric studies.

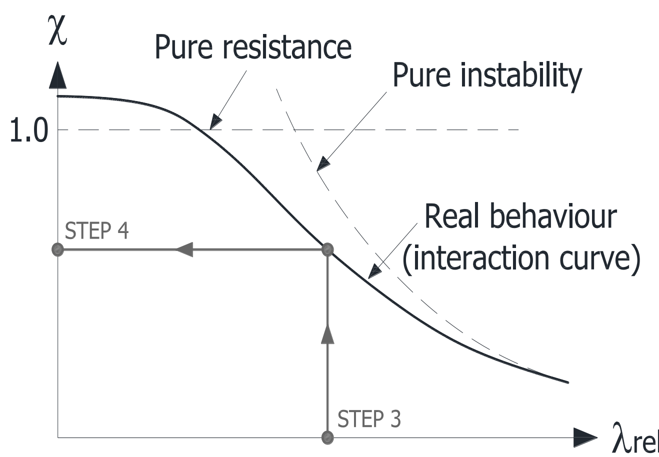

$$STEP\ 1: R_{RESIST}$$

$$STEP\ 2: R_{STAB}$$

$$STEP\ 3: \lambda_{rel} = \sqrt{\frac{R_{RESIST}}{R_{STAB}}}$$

$$STEP\ 4: \chi = f^{\circ}\left(\lambda_{rel}\right)$$

$$STEP\ 5: R_{REAL} = \chi \cdot R_{RESIST}$$

Figure 1 : Application steps of the OIC

2. Experiments on hollow structural shapes

In order to examine the cross-sectional behavior of structural hollow sections, an experimental program was carried out on a wide variety of cross-sectional shapes (RHS, SHS, CHS) with different dimensions and local plate slenderness in order to investigate the influence of local buckling on the plastic, elastic-plastic or slender cross-section capacity of tubular sections. The main aim of this test campaign is to provide an experimental reference to assess numerical FEM models.

The testing program comprised 57 tests involving twelve different section shapes:

- RHS 200x100x4, S355, cold-formed;

- RHS 220x120x6, S355, cold-formed;
- RHS 250x150x5, S355, hot-finished;
- RHS 200x100x5, S355, hot-finished;
- SHS 200x200x5, S355, hot-finished;
- SHS 200x200x5, S355, cold-formed;
- SHS 200x200x6, S355, cold-formed;
- SHS 200x200x6.3, S355, hot-finished;
- CHS 156x6.3, S355, hot-rolled;
- CHS 159x6.3, S355, cold-formed;
- CHS 159x5, S355, hot-rolled;
- CHS 159x7.1, S355, hot-rolled.

Nine 3 m long beams and three 6 m long beams (i.e. a total of twelve beams) were delivered at the Structural Engineering lab of the University of Applied Sciences of Western Switzerland – Fribourg. Each beam was divided into 700 mm length short specimens and pieces of each parent beam were kept for the residual stress measurements, tensile tests coupons and stub column testing.

Measurements of cross-sectional dimensions and of geometrical imperfections were made, and tensile tests were carried out to determine the material stress-strain behavior. Stub column tests were also performed for all different cross-section types. As for the main cross-sectional tests, six load cases (LC) were distinguished. Mono-axial and bi-axial bending with axial compression load cases were considered through the application of eccentrically-applied compression forces. Different M/N ratios have been adopted, in order to vary the distribution of stresses on the flanges and webs, thus the failure modes were as follows:

- LC1: pure compression N;
- LC2: major-axis bending M_y (50%) + axial compression N (50%)1;
- LC3: bi-axial bending M_y (33%) + M_z (33%) + axial compression N (33%);
- LC4: minor-axis bending M_z (50%) + axial compression N (50%);
- LC5: bi-axial bending M_y (25%) + M_z (25%) + axial compression N (50%);
- LC6: bi-axial bending M_y (10%) + M_z (10%) + axial compression N (80%).

2.1 Material property tests

The stress-strain behavior of the tested specimens was determined through 55 tensile tests. For each of the eight SHS and RHS parent elements, four necked coupons were cut from each flat face. The coupons were 270 mm long. In addition, two straight corner coupons were also extracted and tested for each of these eight sections in order to investigate the increase in strength in the cold-formed corners and to confirm uniform properties in the hot finished corners (Figure 2). All coupons were extracted in the longitudinal direction of the specimens. As for the

CHS specimens, two coupons were extracted from each section. The corners coupons were 150 mm long with cross-sections dimensions of 3 mm x 3 mm cut inside the cross-section thicknesses in order to avoid creating eccentric applied loads while testing. The stresses were calculated on the basis of the applied force and the real cross-section of each coupon measured before testing. However, for the corner coupons, the area was also determined by dividing its weight by its initial length and density.

Typical stress-strain curves measured from hot-rolled and cold-formed material are shown in Figure 3. The hot-finished material law is clearly displaying the sharply defined yield point with the yield plateau followed by a subsequent strain-hardening, whilst the cold-formed material law is showing a more rounded response. The test results from the flat coupons and corner coupons are summarized in Table 1.

Table 1 : Material properties of flat and corner tensile coupons

Base profile*	Position [mm]	E [N/mm^2]	f_y [N/mm^2]	ε_y [%]	f_u [N/mm^2]	ε_u [%]
RHS 200x100x5_HF	Flat	215000	420	0.21	520	18
	Corner	210000	418	0.18	520	15
RHS 250x150x5_HF	Flat	212000	447	0.21	576	18
	Corner	211000	435	0.3	535	12
SHS 200x200x6.3_HF	Flat	215000	452	0.2	496	16
	Corner	210000	487	0.3	523	8
SHS 200x200x5_HF	Flat	211000	475	0.23	523	15
	Corner	218000	544	0.24	580	9
RHS 220x120x6_CF	Flat	206000	454	0.42	563	16
	Corner	207000	-	-	644	1
RHS 200x100x4_CF	Flat	216000	494	0.42	611	12
	Corner	213000	-	-	601	1.2
SHS 200x200x5_CF	Flat	214000	480	0.42	585	15
	Corner	209000	-	-	573	1.2
SHS 200x200x6_CF	Flat	217000	500	0.43	596	14
	Corner	210000	-	-	620	1.1
CHS 159x7.1_HR	-	212000	442	0.2	557	13
CHS 159x5_HR	-	215000	460	0.2	577	7
CHS 159x6.3_HR	-	213000	460	0.2	673	13
CHS 159x6.3_CF	-	195000	607	0.5	628	1.15

**HF: Hot-finished, HR: Hot-rolled, CF: Cold-formed*

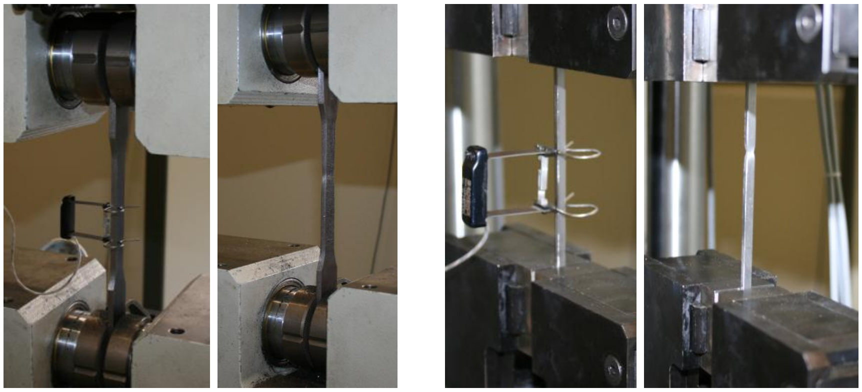

Figure 2 : Flat and corner tensile coupons during testing

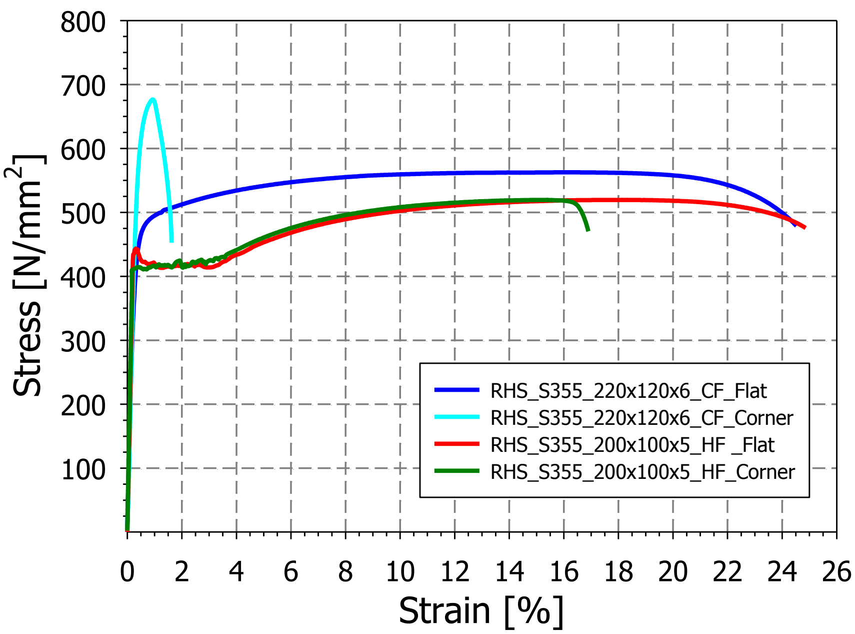

Figure 3: typical Stress strain material law for corner and flat regions of HF and CF sections

It shall be mentioned that the corner coupons where the obtained yield strength is smaller than the corresponded yield strength of the flat coupons is mainly due to the uniform geometry of the cut coupon. In some tests, the stresses were localized in the grips zone and the failure occurred prematurely in this region.

2.2 Residual stresses

The strip-cutting method has been adopted to measure both flexural stresses and membrane residual stresses. It consists in a destructive technique relying on the measurement of strains linked with the release of residual stresses after the cutting of small strips within the cross-section; material relaxation generates either elongation or shortening of the strips due to membrane stresses and a curvature due to flexural stresses, which are linked to the initial residual stresses.

Residual stresses from all twelve parent members were measured; in this respect, a segment of the parent beam was specifically kept to measure residual stresses, and was cut into small strips along the cross section. Prior to cutting, the strips were marked on the cross section by two 100 mm-spaced circular marks, and measurements of length variation were achieved, with an accuracy of +/- 3 mm. The length and the curvature were measured respectively before and after cutting. Hooke's law, along with geometrical equations for the curvature determination was used to get both flexural and membrane residual stresses distributions. Views of the strip-cutting technique are shown in Figure 4. Figure 5 displays an example of the obtained residual stresses patterns for a hot-finished section and a cold-formed section. In the latter section, the flexural residual stresses are seen to be much higher than their membrane counterparts, due to cold-forming effects, whereas the flexural stresses are negligible in the hot-finished section compared to the membrane residual stresses.

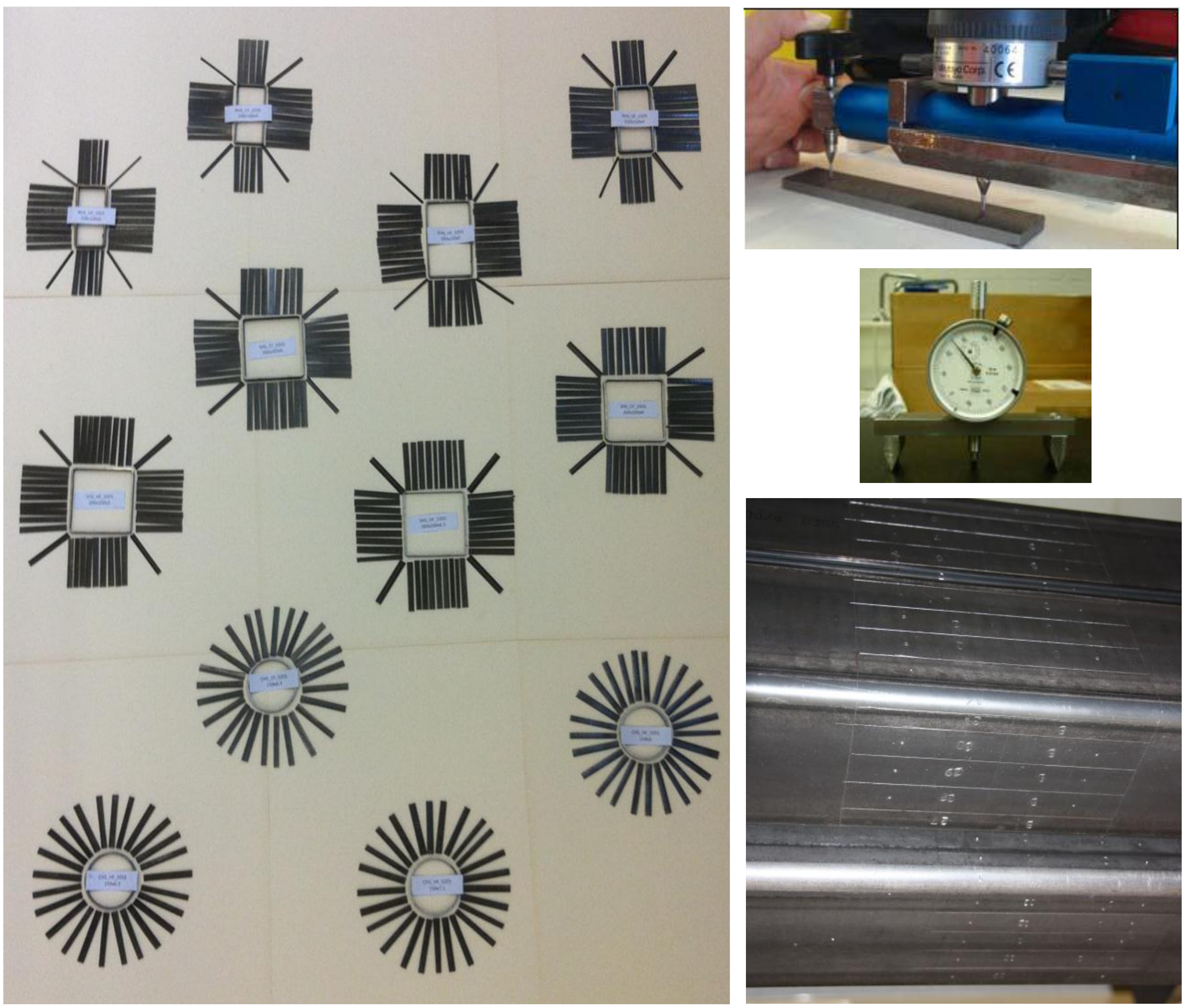

Figure 4: Cross-section strips before and after cutting – measurement devices

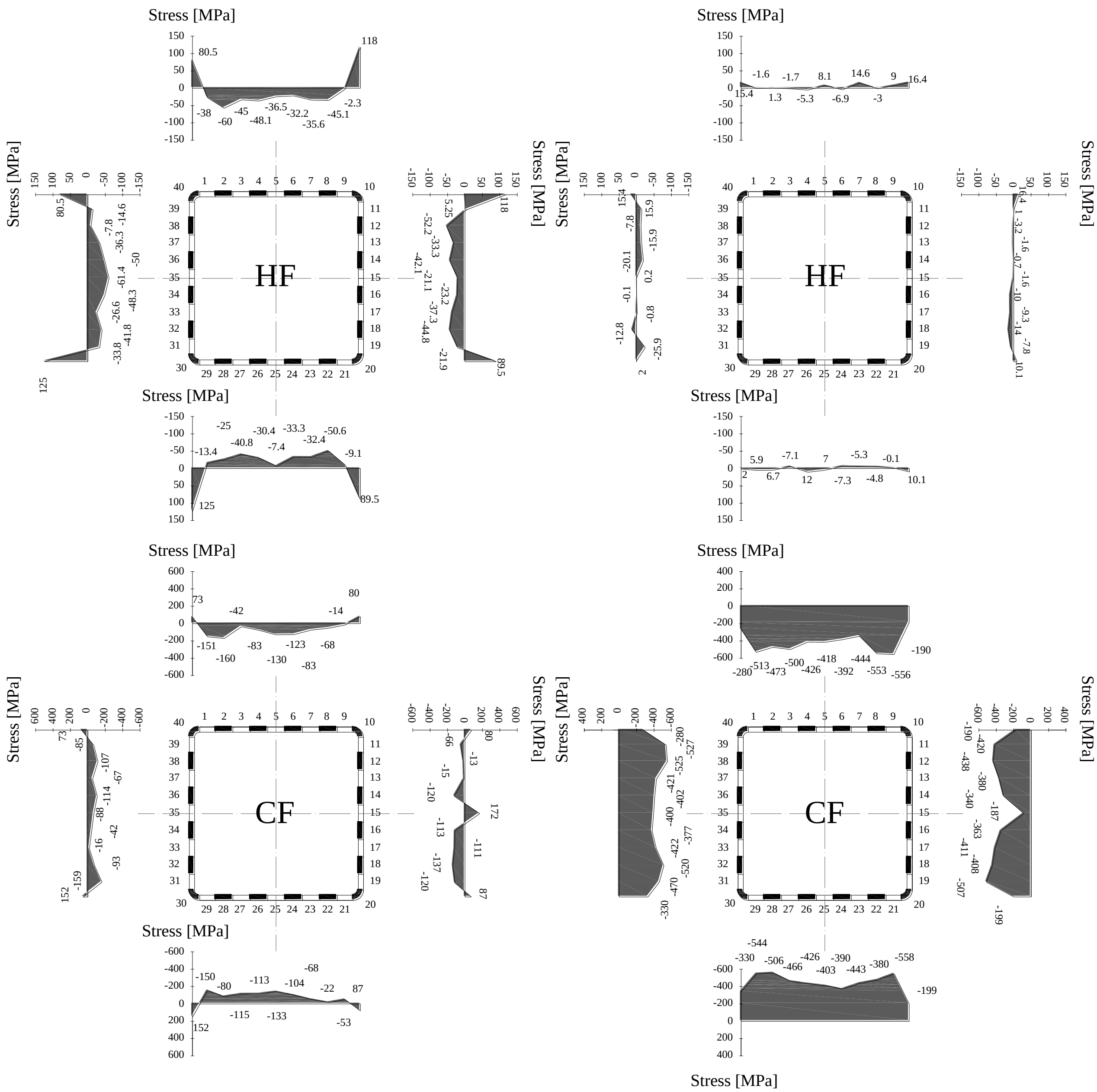

Figure 5: Measured flexural (right column) and membrane (left column) of a hot-finished specimen SHS_HF_200x200x6.3 (first line) and a cold formed specimen SHS_CF_200x200x6 (second line)

2.3 Measurement of geometrical imperfections

Measurement of geometrical imperfections was made by means of an aluminum perforated bar containing 9 equally-spaced variable displacement transducers (LVDTs) which was displaced sideways on each specimen's plate in order to get 3D geometrical plate representations; after having measured all faces of a specimen, all information have been gathered in a recomposed specimen that contains the measured local geometrical imperfections (Figure 7). The objective is here to provide accurate data for the FE models in a later stage of the investigations. The aluminum bar supporting the LVDTs was designed so as to be able to move the LVDTs themselves within the bar, and to let the possibility to adjust the position according to the desired height corresponding to the end plate dimensions. An example of the measurement procedure of local imperfections is shown below, along with the general imperfect shapes of a cross-section.

Figure 6: Geometrical imperfection measurement – LVDTs detail bar

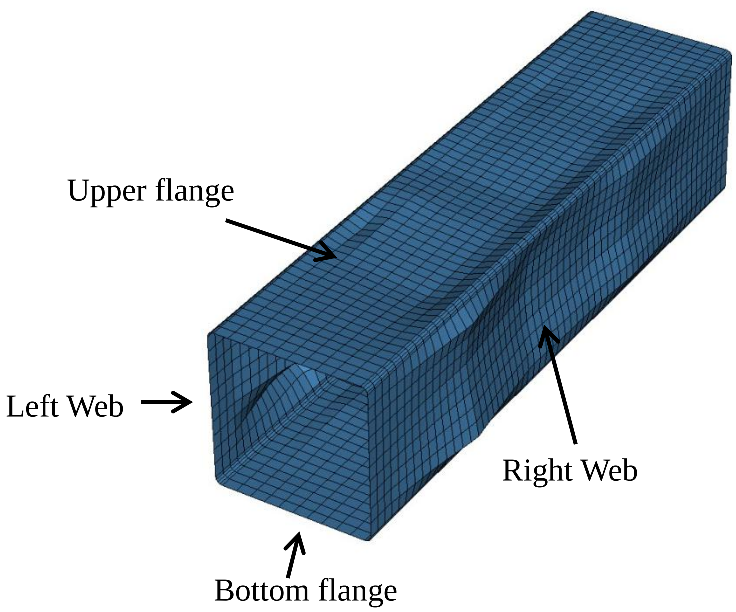

Figure 7: 3D amplified imperfect shape of the specimen SHS200x200x6.3 (x15)

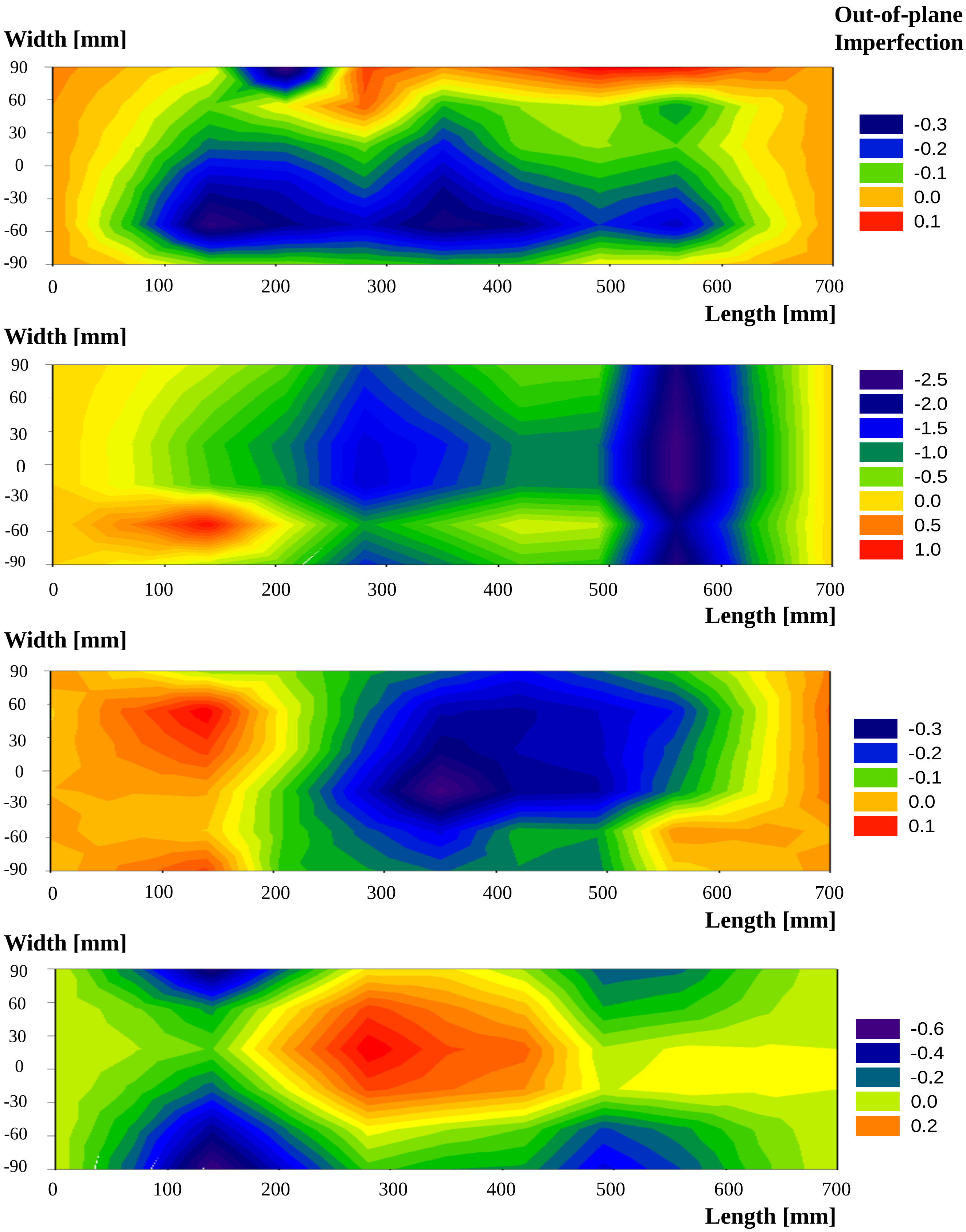

Figure 8: Imperfect plates of the SHS200x200x6.3 (upper flange, left web, bottom flange, right web respectively)

2.4 Stub column tests

12 stub column tests were performed for each cross-section type. The length of each stub column was chosen in a way that measures about three times the height of the cross section, in an attempt to avoid global buckling. The cross-section dimensions were measured at both ends repeatedly using a digital micrometer. Moreover, the length and weight of each specimen were measured prior to testing, and used later on for the calculation of the measured area assuming a density of 7850 kg/m^3 .The flatness and parallelism of the faces have been checked for each column prior to testing using a flat marble stone. Two strain gauges have been attached at mid-height of all the elements after polishing and cleaning the surface. The stub column resulted in an average stress-strain curve of the actual profile and were performed using a 5000 kN hydraulic testing machine. Two plates with increased hardness have been attached to each side of the stub columns in order to protect the testing machine surface. Four LVDTs were used in order to record the average end-shortening behavior.

During the test, the strains were monitored live to ensure that, not only compression was kept concentrically-applied but, also to check the load displacement behavior of the specimen in the elastic range in order to assess the corresponding Young's modulus. For stocky sections, typical failure occurred with a whole cross-section yield with local buckling at the ends of the specimens, whilst for slender sections, local buckling was located at the middle of the specimen. The measured ultimate loads F_{exp} of the tested specimens are listed in Table 2. The failure shapes of all stub columns along the experimental test set up are shown in Figure 9.

Figure 9: General test set-up and failure shapes of the stub columns

The end shortening measurements from the displacement transducers were different from the strains registered from the strain gauges. A correction method described by the Centre for Advanced Structural Engineering (Rasmussen& Hancock 1993, Rasmussen 2000) was used, which combined both sets of measurements because the strain gauges provide the correct initial Young's modulus slope as they were directly in contact with the column faces, but they give less useful information when influenced by local buckling. Whereas, the LVDTs provide good post-yield information but pick up the stiffness of the end plates leading to an incorrect initial stiffness. The method consists of a correction factor k representing the unwanted displacement, which is then deduced from the end displacement. Figure 10 shows an example of two load displacement curves, before and after the correction of the corresponding slopes.

$$k = \frac{L}{2}\left(\frac{1}{E_{LVDT}} - \frac{1}{E_{SG}}\right) \tag{1}$$

$$\delta_c = \delta_{LVDT} - 2kf \tag{2}$$

Where E_{LVDT} represents the initial Young's modulus calculated from the LVDT readings and E_{SG} represents the initial Young's modulus calculated from the strain gauges. f represents the applied stress.

Table 2 : Measured properties and ultimate loads of stub columns

Base profile	M [kg]	L [mm]	Area [mm^2]	N_y [kN]	N_{exp} [kN]	N_{exp} / N_y [-]
RHS_S355_CF_200x100x4	10.3	600	2186	1080	761	0.70
RHS_S355_CF_220x120x6	19.6	681	3675	1669	1648	0.98
RHS_S355_HF_250x150x5	23	700	4167	1863	1358	0.72
RHS_S355_HF_200x100x5	13.4	600	2855	1199	1163	0.96
SHS_S355_CF_200x200x5	17.3	599	3676	1765	1296	0.73
SHS_S355_CF_200x200x6	20.5	599	4356	2178	1957	0.89
SHS_S355_HF_200x200x5	17.1	600	3620	1720	1607	0.93
SHS_S355_HF_200x200x6.3	21.5	600	4575	2068	2227	1.07
CHS_S355_CF_159x6.3	10.8	481	2870	1742	1800	1.03
CHS_S355_HR_159x6.3	11.8	480	3132	1441	1560	1.08
CHS_S355_HR _159x5	9.2	480	2454	1129	1255	1.11
CHS_S355_ HR _159x7.1	12.4	480	3291	1454	1632	1.12

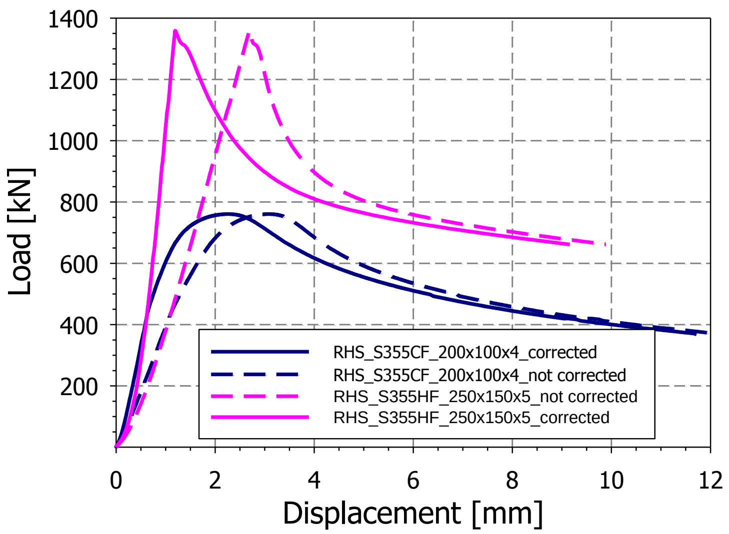

Figure 10: Load displacement curve correction

2.5 Cross-sectional tests

The mono-axial and the bi-axial-bending with axial compression load cases were obtained through applying compression eccentrically. End-plates were welded to the profiles with different eccentricities, according to the desired load case. All tests were performed in the Structural Engineering laboratory of the University of Applied Sciences - Fribourg. The response of each test has been carefully monitored and recorded, in view of the validation of Finite Element models. The end plates and the loading plates had respectively a thickness of 20 mm and 40 mm in order to apply the loading evenly on the ends of the specimen. Measurements were made for end plates shortening and end plates rotations at both extremities. All cross-section tests have been carried out in a testing machine of 4000 kN max capacity. The general set-up is shown in Figure 11.

All the local buckling failure modes are represented in Figure 12. The measured maximum forces of the hot-rolled tested specimens are listed in Table 3.

Figure 11: General test set-up of cross-section tests

LC1

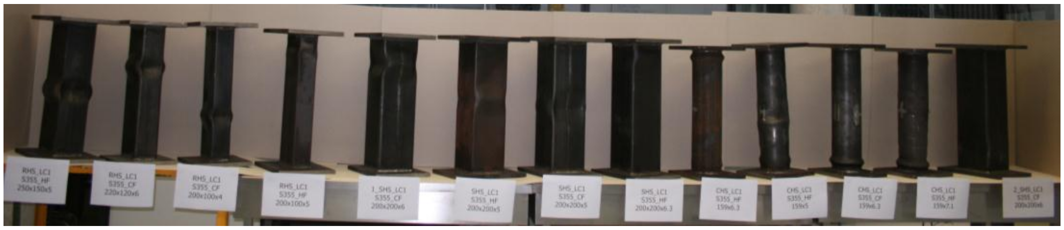

LC2

LC3

LC4

LC5

LC6

Figure 12: Failure shapes of all cross-sections tests

All tests had pinned end conditions with all rotational degrees of freedom being free. However, to avoid torsional rigid body movements of the specimen, the specially designed hinges have been restrained against torsional rotation, except for the loading cases of compression and biaxial bending, where this was not possible.

 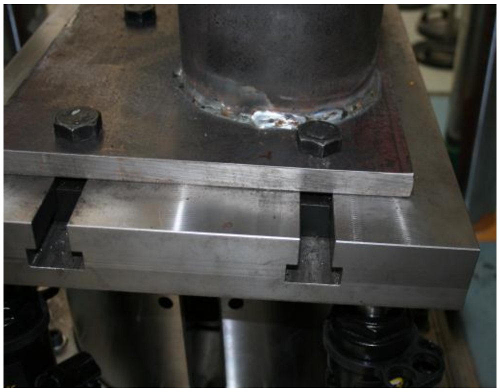

Figure 13: Hinge details

Table 3 : Ultimate experimental loads of hot-finished cross-section tests

Base profile	Load case [-]	e_y_e_z* [mm]-[mm]	F_{exp} [kN]
RHS_LC1_S355_HF_250x150x5	N (100%)	0_0	1478
RHS_LC1_S355_HF_200x100x5	N (100%)	0_0	1159
SHS_LC1_S355_HF_200x200x5	N (100%)	0_0	1604
SHS_LC1_S355_HF_200x200x6.3	N (100%)	0_0	2168
RHS_Stub_S355_HF_250x150x5	N (100%)	0_0	1359
RHS_Stub_S355_HF_200x100x5	N (100%)	0_0	1163
SHS_Stub_S355_HF_200x200x5	N (100%)	0_0	1607
SHS_Stub_S355_HF_200x200x6.3	N (100%)	0_0	2227
RHS_LC2_S355_HF_250x150x5	N (50%) + M (50%)	0_47	1063
SHS_LC2_S355_HF_200x200x5	N (50%) + M (50%)	60_60	942
SHS_LC2_S355_HF_200x200x6.3	N (50%) + M (50%)	50_50	1302
RHS_LC3_S355_HF_250x150x5	N (33%) + M (33%) + M (33%)	46_78	623
RHS_LC3_S355_HF_200x100x5	N (33%) + M (33%) + M (33%)	25_48	589
SHS_LC3_S355_HF_200x200x5	N (33%) + M (33%) + M (33%)	0_62	828
SHS_LC3_S355_HF_200x200x6.3	N (33%) + M (33%) + M (33%)	0_60	1069

*e_y represents the adopted eccentricity along y-y axis, e_z is the adopted eccentricity along z-z axis

3. Numerical Investigation

3.1 Modeling assumptions

Extensive series of numerical computations have been performed with the use of non-linear FEM software FINELg, continuously developed at the University of Liège and Greisch Engineering Office since 1970. This software offers almost all types of FEM types of analyses, and present investigations have mainly been resorting to so-called MNA (Materially Non-linear Analysis), LBA (Local Buckling Analysis) and GMNIA analyses. The cross-sections were modeled with the use of quadrangular 4-nodes plate-shell finite elements with typical features (corotational total Lagrangian formulation, Kirchhoff's theory for bending). The corners of square and rectangular profiles were modeled with 4 linear shell elements per corner.

Averaged measured geometrical dimensions were used in the calculations along with measured local imperfections for each specimen. Measured membrane stresses were introduced for the hot-finished profiles, whereas both measured flexural and membrane stresses were introduced for cold-formed profiles. Figure 14 displays an example of the adopted measured membrane stresses for specimen SHS_HF_200x200x6.3.

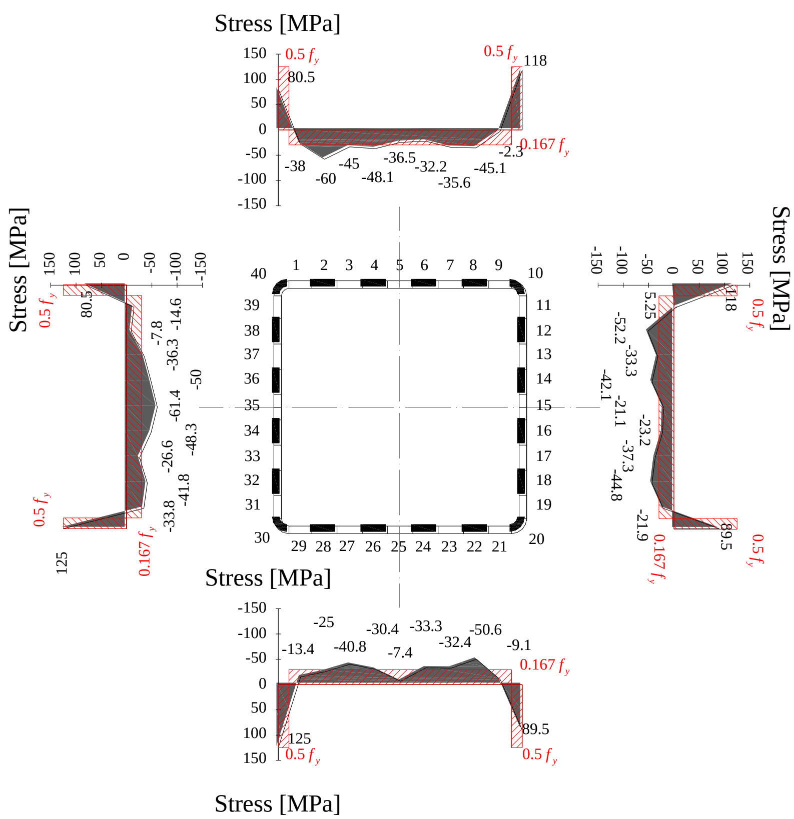

Figure 14: Adopted measured membrane stresses for section SHS_HF_200x200x6.3.

Averaged material stress-strain behavior including hardening effects was included. For the cold-formed tubular profiles, two material laws have been defined – one for the base material and one for the corner regions – using the Ramberg-Osgood material law. Accordingly, a higher yield strength in the cold-formed corner regions was taken into account.

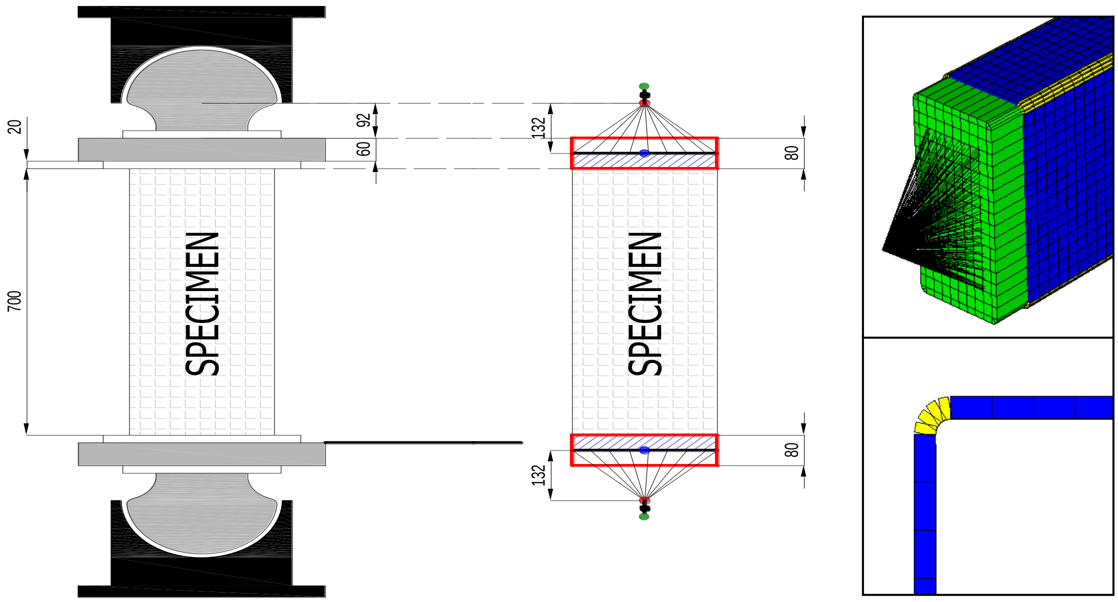

Figure 15: Finite element model assumptions

In order to represent accurately the experimental behavior of the specimens, a suitable FE-model had to be developed. Specimens have been modeled with a regular mesh. The endplates were represented through rigid plates having an equivalent thickness of 80 mm and modeled with shell elements that remain elastic during loading. The plates' stiffness allowed an even distribution of the applied load at the ends of the sections and prevented the cross-sectional deformation at both ends while allowing free rotations. As for the behavior of the hinges, truss elements were used to simulate the rigid spherical hinges at both ends. All trusses were connected to the rigid end plates nodes and to the centroid of the hinge. The load was applied at the centroid of the hinge, and the cases with strong axis and biaxial bending moment were represented though an axial load applied to the centroid of the hinge with the correspondent measured eccentricities from the cross-section tests (Figure 15).

3.3 Validation

The experimental and numerical cross-section capacities achieved by the specimens tested were compared. The ultimate loads and the ratio of the numerical ultimate loads versus experimental ultimate load are given for the hot-finished square and rectangular sections in Table 4 (stubs, LC1, LC2, and LC3). As previously mentioned, all numerical simulations of the specimens were based on actual cross-sectional dimensions and on actual material properties. Numerical simulations represented the real behavior quite accurately (Table 4). The differences between numerical and experimental results are mainly due to testing uncertainties such as a little friction in the hinges, small inconsistencies in the imperfections measurements and load eccentricities.

A graphical comparison of the ultimate loads of the FE-simulations and of the experiments is shown in Figure 16 in which the red lines indicate a deviation of +/- 10%. It can be seen that all numerical simulations are in good accordance with the test results. All other values oscillate very closely around the continuous line, which indicates a very good accordance between test results and numerical results.

Table 4: Comparison of numerical and experimental ultimate loads

Base profile	Load case [-]	F_{FEM} [kN]	F_{exp} [kN]	F_{exp}/F_{FEM} [-]
RHS_LC1_S355_HF_250x150x5	N (100%)	1508	1478	0.98
RHS_LC1_S355_HF_200x100x5	N (100%)	1145	1159	1.01
SHS_LC1_S355_HF_200x200x5	N (100%)	1606	1604	1.001
SHS_LC1_S355_HF_200x200x6.3	N (100%)	2145	2168	1.01
RHS_Stub_S355_HF_250x150x5	N (100%)	1386	1359	0.98
RHS_Stub_S355_HF_200x100x5	N (100%)	1163	1163	1.00
SHS_Stub_S355_HF_200x200x5	N (100%)	1612	1607	0.99
SHS_Stub_S355_HF_200x200x6.3	N (100%)	2193	2227	1.01
RHS_LC2_S355_HF_250x150x5	N (50%) + M (50%)	1053	1063	1.01
SHS_LC2_S355_HF_200x200x5	N (50%) + M (50%)	935	942	1.01
SHS_LC2_S355_HF_200x200x6.3	N (50%) + M (50%)	1274	1302	1.02
RHS_LC3_S355_HF_250x150x5	N (33%) + M (33%) + M (33%)	654	623	0.97
RHS_LC3_S355_HF_200x100x5	N (33%) + M (33%) + M (33%)	590	589	0.99
SHS_LC3_S355_HF_200x200x5	N (33%) + M (33%) + M (33%)	811	828	1.02
SHS_LC3_S355_HF_200x200x6.3	N (33%) + M (33%) + M (33%)	1076	1069	0.99

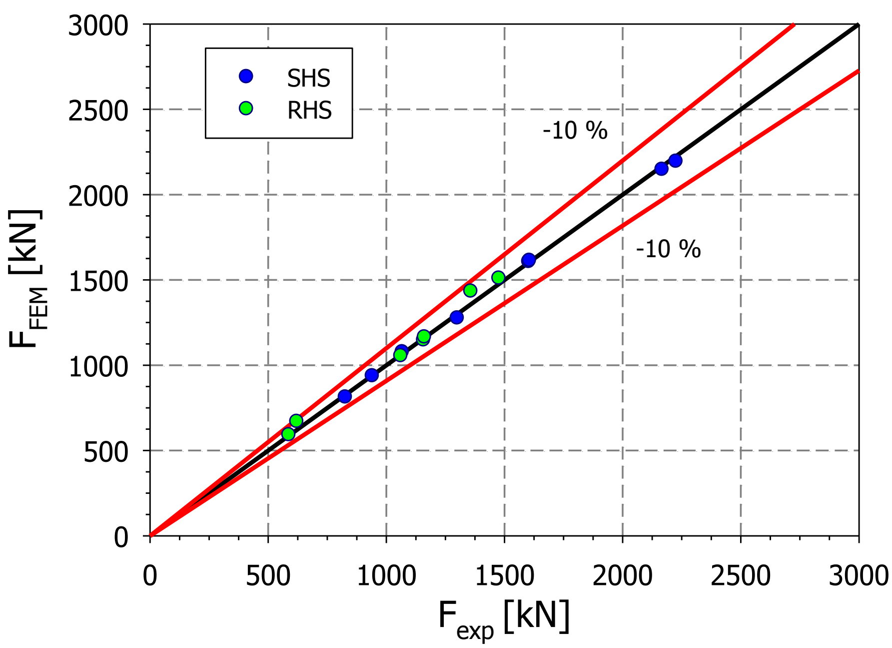

Figure 16: FE numerical loads vs. ultimate experimental loads

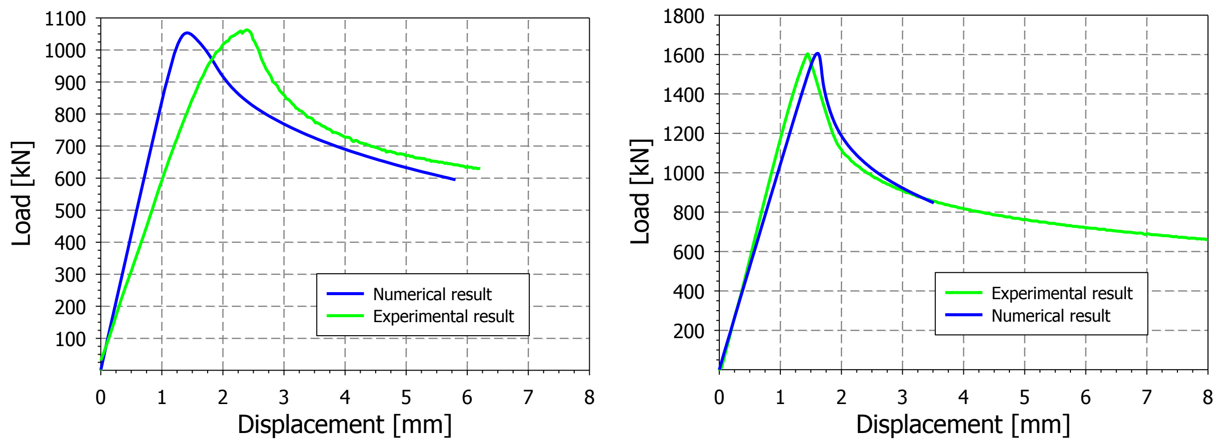

Figure 17: Numerical vs. experimental load displacement curves of specimens: RHS_LC2_250x150x5_HF (left), SHS_Stub_200x200x5_HF (right)

Based on these comparisons, which comprise a lot of representative load cases and different cross-section slenderness, the applied finite element modeling of the specimens can be accepted scientifically. Even if another finite element model – similar to the one referred – will be adopted in parametric studies, it was shown to be a suitable finite element model and the derived numerical tests can be used as basis for further code developments.

5. Conclusions – Future developments

In the present paper, an experimental test program on rectangular, square and circular hollow sections of grade S355 structural steel (50 ksi) steel was reported. Hot-finished, hot-rolled and cold-formed stub columns and cross-section tests with various load cases (pure compression, compression and strong axis-bending, compression and weak-axis bending, compression and biaxial bending) were described. Moreover, the secondary measurements were recorded and consisted in tensile tests, imperfection and residual stress measurements.

The tensile coupons tests clearly showed the sharply defined yield plateau for hot-finished and hot-rolled sections, the rounded response of the cold-formed sections and the increase in strength in the corners regions of these cold-formed sections. Also, the corresponding yield stresses were 20 to 30% higher than the nominal values of the hot-formed and hot-finished sections, and higher than 35% for the cold-formed sections.

The residual stress measurements were done through the sectioning technique; flexural stresses were seen to be much higher than the membrane stresses in the cold-formed sections, whereas the hot-finished and hot-rolled sections had much higher membrane stresses compared to the flexural stresses.

The experimental and numerical cross-section capacities achieved by the specimens tested were compared. A numerical model was developed to represent the hinges end conditions and the plates of the experimental tests. Suitable measured material laws for hot-finished, hot-rolled and cold-formed sections were used (i.e. Elastic-perfectly plastic with 2% strain hardening for hot-formed and hot-rolled sections and Ramberg-Osgood material law for the cold formed with an increase in yield strength for the corners). The measured imperfections and measured residual stresses were also introduced. Numerical simulations represented the real behavior quite accurately. The numerical results were in a very accordance with the experimental results.

A second part of the study will follow and will consist of numerical parametric studies on hot-rolled and cold-formed hollow sections, used to address precise and suitable interaction curves capable of describing the cross-sectional behavior of tubular sections. Furthermore, O.I.C. based investigations on the member ultimate and rotation capacity of tubular sections are currently under way and represent continuity and complementary studies on the derivation of accurate and well-designed formulae, which support the Overall Interaction Concept.

Acknowledgements

The authors would like to thank the engineers and technicians of the structural laboratory of Civil Engineering of the University of Applied sciences of Western Switzerland – Fribourg, and Voestalpine Krems, Austria for the supply of the test members

References

AISC (2005). Specification for structural steel buildings. American Institute of Steel Construction, Chicago, IL. ANSI/ASIC 360-05.

Bebiano R., Pina P., Silvestre N. and Camotim D. (2008). "GBTUL – Buckling and Vibration Analysis of Thin-Walled Members", DECivil/IST, Technical University of Lisbon (http://www.civil.ist.utl.pt/gbt).

Boissonnade N. (2011). "The Concept of Cross-section Classes in Eurocode 3 into Question", ECCS TC8 meeting, Lisbon, June 3rd.

Boissonnade N., Greiner R., Jaspart J.P., Lindner J. (2006) "Rules for Member Stability in EN 1993–1–1; Background documentation and design guidelines", Eds. Mem Martins, Portugal, E.C.C.S. – ISBN 92-9147-000-84, Vol. 119, 259 pages.

Boissonnade, N. & Somja, H. 2012. "Influence of Imperfections in FEM Modeling of Lateral Torsional Buckling". *Proceedings of the Annual Stability Conference, Structural Stability Research Council*, Grapevine, Texas, April 18-21BSI British Standards Institution (2000) BS5950. The Structural Use of Steelwork in Building: Part 1: Code of Practice for Design: Rolled and Welded Sections, BSI, London.

CEN (Comité Européen de Normalisation) (2005). "Eurocode 3: Design of Steel Structures, Part 1–1: General rules and rules for buildings (EN 1993-1-1)", Brussels.

CEN (Comité Européen de Normalisation) (2005). "Eurocode 3: Design of Steel Structures, Part 1–5: Design of plated structures (EN 1993-1-1)", Brussels.

DIN 18800 1-4: 1990 (1990). "Stahlbauten." *Beuth Verlag GmbH*, Berlin.

Gardner, Leroy (2008). "The continuous strength method". Proc. Institution of Civil Engineers: Structures and Buildings, vol. 161, n°3, p 127-133.

Gardner L., Wang F., Liew A. (2011). "Influence of strain hardening on the behavior and design of steel structures", *International Journal of Structural Stability and Dynamics*, Vol. 11, pp. 855-875.

Kettler M. (2008). "Elastic-plastic cross-sectional resistance of semi-compact H- and hollow sections". *PhD Thesis*, Graz Technical University.

Li Y., Rossi B. (2012). "Finite element model for the extension of the Direct Strength Method to hot-rolled profile cross-sections", Proc. of the Nordic Steel Construction Conference, Oslo, Norway, 5-7 September.

Li Z., Schafer B. (2010) "Buckling analysis of cold-formed steel members with general boundary conditions using CUFSM: conventional and constrained finite strip methods." Proceedings of the 20th Int.. Spec. Conf. on Cold-Formed Steel Structures, St. Louis, MO. November, 2010.

Maquoi R., Rondal J. (1978). "Mise en équation des nouvelles courbes européennes de flambement", Construction Métallique, n°1, pp. 17-30.

Massonnet C. (1976). "Forty Years of Research on Beam-Columns in Steel", *Solid Mechanics Archives*, Noordhoff International Publishing, Leyden, Vol.1, n°1.

Merchant, W. (1954). "The failure load of rigid jointed frameworks as influenced by stability", *The Structural Engi neer*, 32, No. 7, July, pp. 185–90.

Non-linear finite element analysis program "FINELg" (2012), *User's Manual, version 9.3*, ArGEnCo Department, University of Liège, Greisch Info S.A., Liège, Belgium.

Ofner R. (1997) "Traglast von Staben aus Stahl bei Druck und Biegung". *PhD Thesis*, Graz Technical University.

"Plastic member capacity of semi-compact steel sections – a more economic design (Semi-Comp)" (2007). *Final report (01/01/06 – 30/06/07)* – RFCS – Steel RTD (Contract RFS-CR-04044).

Rasmussen K.J.R. & Hancock "Design of cold-formed Stainless Steel Tubular Members I:columns", *Journal of Structural Engineering, Americal Society of Civil Engineers*, Vol. 119, 1993, pp 2349-2367

Rasmussen K.J.R. & Hancock "Design of cold-formed Stainless Steel Tubular Members II: Beams*", Journal of Structural Engineering, Americal Society of Civil Engineers*, Vol. 119, 1993, pp 2368-2386

Rasmussen K.J.R."Recent Research on Stainless steel Tubular structures", *Journal of Structural Engineering*, Vol. 54, No. 1, 2000, pp 75-88.

Schafer B. (2006). "Cross-section Stability of Structural Steel", AISC Faculty Fellowship Research Project.

Seif M., Schafer B. (2010). "Local buckling of structural steel shapes", *Journal of Constructional Steel Research*, vol. 66, pp. 1232-1247.

S.T.S.S. (2012). "Research project STSS – Simple Tools Sell Steel" (http://www.ims.org/2012/02/stss-simple-tools-sell-steel/).

Ziemian, R., McGuire W. (2009). MASTAN2, www.mastan2.com.